RSC Advances

PAPER

View Article Online
View Journal | View Issue

Cite this: *RSC Adv.*, 2025, **15**, 11799

Mechanistic insights on the Lewis acid-catalyzed three-component cationic Povarov reaction: synthesis of *N*-propargyl 1,2,3,4-tetrahydroquinolines†

Yeray A. Rodríguez-Núñez, *[a] Jesús Sánchez-Márquez, [b] Jorge Quintero-Saumeth, [f] Cristian J. Guerra, [c] Efraín Polo-Cuadrado, [d] David Villaman, [e] Cristopher A. Fica-Cornejo [a] and Arnold R. Romero Bohórquez *[f]

In this study, the Povarov cationic reaction mechanism was explored using five different Lewis acids as catalysts for the synthesis of *N*-propargyl-6-methoxy-4-(2′-oxopyrrolidin-1′-yl)-1,2,3,4-tetrahydroquinoline, where the best reaction yield was obtained using $InCl_3$. The desired product was not obtained in the absence of a catalyst. A comprehensive theoretical analysis at the density functional theory (DFT) level was conducted to study the role of the catalyst and establish a detailed reaction mechanism. Electron localization function (ELF) analyses were performed to elucidate the key bonding events during the reaction stages, highlighting the differences in bond formation among the different catalysts. Our results showed that the presence of an acid catalyst is required for obtaining the intermediary iminium ion. In this sense, the $InCl_3$ catalyst provides the lowest energy barrier for catalytic interactions, increasing the electrophilic character and, therefore the reactivity of formaldehyde, promoting the formation of iminium ions and subsequently triggering the obtaining of the tetrahydroquinoline compound. In fact, from theoretical analysis, our findings provide evidence of the formation of the tetrahydroquinoline compound through a set of energetically favorable step reactions, ruling out a concerted process. The step involved in this part of the mechanism includes the formation of a Mannich-type adduct, obtained by the nucleophilic addition reaction between the iminium cation and an activated alkene, and a subsequent cyclization *via* an intramolecular Friedel–Crafts reaction. This defines the cationic Povarov reaction as a domino reaction and invites us to discard the wrong use of the name Aza Diels–Alder or imino Diels–Alder for this type of reaction.

Received 26th February 2025
Accepted 10th April 2025

DOI: 10.1039/d5ra01375e

rsc.li/rsc-advances

Introduction

N-heterocyclic compounds of both natural and synthetic origin are of great interest in synthetic and medicinal chemistry because most small molecules have remarkable pharmacological effects and contain at least one nitrogen atom in their structure.[1] Among these *N*-heterocycles, quinolines and their partially reduced derivatives, tetrahydroquinolines (THQs), stand out due to their ubiquity and bioactive profile. Several studies have documented the presence of tetrahydroquinoline scaffolds in the molecular structure of biologically interesting natural products and pharmaceutical agents. The biological activities attributed to these derivatives include antimalarial,[2] antioxidant,[3] antifungal,[4] antitumor,[5] and antileishmanial[6] activities.

Considering the pharmacological applications of tetrahydroquinolines and the growing interest in accessing new and promising derivatives based on these compounds, several

[a]*Universidad Andrés Bello, Facultad de Ciencias Exactas, Departamento de Ciencias Químicas, Laboratorio de Síntesis y Reactividad de Compuestos Orgánicos, Santiago 8370146, Chile. E-mail: yeray.rodriguez@unab.cl; c.ficacornejo@uandresbello.edu*

[b]*Departamento de Química-Física, Facultad de Ciencias, Campus Universitario Río San Pedro, Universidad de Cádiz, Cádiz, Spain*

[c]*Departamento de Ciencias Químicas, Facultad de ciencias Exactas, Universidad Andrés Bello, Republica 275, Santiago, Chile. E-mail: c.guerramadera@uandresbello.edu*

[d]*Departamento de Química Orgánica, Facultad de Ciencias Químicas, Universidad de Concepción, Concepción, Chile. E-mail: epolo@udec.cl*

[e]*Laboratorio de Química Inorgánica y Organometálica, Departamento de Química Analítica e Inorgánica, Facultad de Ciencias Químicas, Universidad de Concepción, Edmundo Larenas 129, Casilla 160-C, Concepción 4070386, Chile. E-mail: dvillaman@udec.cl*

[f]*Grupo de Investigación en Compuestos Orgánicos de Interés Medicinal CODEIM, Parque Tecnológico Guatiguará, Universidad Industrial de Santander, Piedecuesta 681011, Colombia. E-mail: arafrom@uis.edu.co*

† Electronic supplementary information (ESI) available. CCDC 2415596. For ESI and crystallographic data in CIF or other electronic format see DOI: https://doi.org/10.1039/d5ra01375e

synthetic strategies based on classical reactions have been developed. These advances have enabled rapid and efficient access to the tetrahydroquinoline structure, even with high structural functionalization.[7] Some examples of these reactions involve the catalytic reduction of the quinoline core at high hydrogen pressures[8] and intramolecular reactions leading to ring closure, such as aza-Michael–Michael addition,[9] Friedel–Crafts reaction,[10] nucleophilic substitutions (SN), and sigmatropic rearrangements.[11] Nevertheless, owing to its high efficiency and facile performance, the most powerful synthetic tool for the construction of the tetrahydroquinoline skeleton is the acid-catalyzed three-component Povarov reaction. This chemical reaction was first characterized as occurring between primary arylamines and aldehydes (or ketones) to obtain an intermediate arylimine that reacts with electron-rich olefins in the presence of an acid catalyst *via* a formal [4 + 2] cycloaddition reaction.[12]

The Povarov reaction mechanism has been the subject of extensive scientific research. Indeed, for decades, the authors have defined Povarov synthesis as an inverse electron-demand aza-Diels–Alder reaction, with the subsequent transfer of protons that leads to the formation of the tetrahydroquinoline core.[13] In this context, the first theoretical study of this mechanism using DFT involves the formation of tetrahydro-1,5-naphthyridine derivatives under acid catalysis, suggesting that the cycloaddition reaction occurs as an asynchronous concerted process.[14] Subsequently, Domingo *et al.* reported two mechanistic studies on the Povarov reaction based on DFT calculations. Initially, it was suggested that the formation of the tetrahydroquinoline ring could occur through a process that involves the following reaction stages: (i) a Lewis acid-catalyzed aza-Diels–Alder (A-DA) reaction between an *N*-arylimine and nucleophilic ethylene, yielding a formal [4 + 2] cycloadduct and (ii) a stepwise 1,3-hydrogen shift at this intermediate. Nonetheless, the mechanistic implications of the stepwise stage are attributed solely to the acid catalyst being performed by the Lewis acid.[15] While using a Brønsted acid as a catalyst, the authors pointed out that the Povarov reaction mechanism corresponds to a domino process that is initialized by the formation of a cationic intermediate, which undergoes a quick intramolecular Friedel–Crafts reaction[16,17]

In contrast, other experimental studies based on the stereochemistry of THQ obtained from *N*-arylimines under acidic conditions indicated that the mechanism of the Povarov reaction is a stepwise process. From this perspective, the Povarov reaction involves an ionic intermediate before imine activation and nucleophilic attack from an electron-rich alkene.[18] Other reports have suggested that the THQ core obtained from these precursors occurs through a domino reaction beginning with the formation of a Mannich adduct, followed by an intramolecular Friedel–Crafts-type reaction.[19]

In addition, N-substituted THQs were synthesized by reacting secondary arylamines with formaldehyde to obtain a highly reactive intermediate iminium ion. Thus, this reaction reacts with nucleophilic olefins in a one-pot process. Initially, this variant was called the cationic imino Diels–Alder reaction.[20] Similarly, the cationic Povarov reaction resembles the oxa-Povarov reaction for chromone synthesis reported by Taylor and Batey,[21] which involves the reaction between a highly reactive aryl-2-oxazine cationic intermediate generated *in situ* using a Lewis catalyst ($SnCl_4$) and styrene as the electron-rich olefin. Interestingly, Domingo *et al.* studied the oxa-Povarov reaction mechanism using DFT methods and concluded that it occurs along a stepwise mechanism; initially, there is a nucleophilic attack of styrene on the oxonium cationic system (Prins reaction) and a subsequent intramolecular Friedel–Crafts reaction.[16]

The use of *N*-arylanilines as precursors to obtain the desired THQ in high yields *via* *N*-aryl-*N*-alkylmethyleneiminium ions has been reported.[22] In previous studies, we reported a simple one-pot methodology for the synthesis of new derivatives of 4-aryl-3-methyl-1,2,3,4-THQ using aqueous HCl as a catalyst between *in situ*-generated cationic 2-azadienes and arylpropenes (isoeugenol and *trans*-anethole).[23] Hence, this work provides the basis for the most recent theoretical study on the mechanism of the cationic Povarov reaction using DFT methods. Wherein, it is assumed that the formation of the products proceeds by a stepwise mechanism. However, the role of acid catalysts in cationic intermediate formation and the subsequent stepwise mechanism has not been well established. Similarly, Lewis acids ($InCl_3$, BF_3, and $BiCl_3$) have been used in the cationic Povarov reaction between the *N*-allyl/propargyl-*N*-arylymethyleneiminium cation and *N*-vinylpyrrolidone to efficiently generate *N*-allyl/propargyl THQs.[22]

In this work, the three components of the cationic Povarov reaction were carried out using five different Lewis acids as catalysts for the synthesis of *N*-propargyl-6-methoxy-4-(2′-oxopyrrolidin-1′-yl)-1,2,3,4-tetrahydroquinoline **4**. When Lewis acids were employed, the corresponding tetrahydroquinoline core was achieved in moderate and high yields. Herein, we performed a comprehensive theoretical analysis at the DFT level to study the role of the catalyst and establish the detailed mechanism of this reaction. Finally, we conducted a real-space analysis of the electron localization function (ELF) to unravel the key chemical bonding events of both the intermediate iminium ion formation and cyclization stages.

Experimental methodology

Chemistry

All reagents were purchased from Sigma-Aldrich and used without further purification. ^1H and ^{13}C NMR spectra were recorded at 400 and 100 MHz, respectively, on a Bruker Ultrashield-400 spectrometer using $CDCl_3$ as the solvent and TMS as the internal standard. The coupling constant (J) was reported in hertz (Hz). An FT-IR Bruker Tensor 27 spectrophotometer coupled with a Bruker platinum ATR cell was used to obtain IR spectra. Mass spectra were recorded using a Bruker Daltonics ESI-IT Amazon X spectrometer with direct injection, operating in full scan at 300 °C and 4500 V in the capillary. The uncorrected melting point (uncorrected) was determined using an Electrothermal IA9100 melting point apparatus. Compound purification was performed *via* column chromatography using silica gel as a support. Analytical grade solvents were used. A suitable single crystal of the compound was measured using single-crystal X-ray diffraction at room temperature (296 K).

Crystals were obtained by slow evaporation from a saturated MeOH/DCM solution of the compound. Data were collected using a Bruker D8 Venture diffractometer equipped with a PHOTON 100 detector and sealed-tube Mo Kα X-ray source (λ = 0.71073 Å). The measured frames were integrated using the APEX4 package and corrected for absorption effects using SADABS.[24] The molecular structure was solved using the Intrinsic Phasing method with SHELXT[25] and refined by full-matrix least-squares against F^2 using SHELXL.[26] Data reduction, refinement, and visualization were performed at the Olex2 interface,[27] which integrates both programs. All non-hydrogen atoms were refined anisotropically, whereas hydrogen atoms were positioned geometrically, fixed with isotropic parameters, and refined with riding coordinates.

The synthesis of *N*-propargyl-4-methoxyaniline 1

Anhydrous dimethyl formamide (DMF, 10 mL), 4-methoxyaniline (10 mmol), sodium carbonate (Na_2CO_3, 11 mmol), and potassium iodide (KI, 0.5 mmol) were added to a round-bottom flask and stirred until complete homogenization. The reaction mixture was then placed in an ice bath at 0 °C for 10 min. Subsequently, a solution of propargyl bromide in DMF (10 mmol) was added dropwise, and the mixture was constantly stirred at room temperature. The reaction was monitored using thin-layer chromatography (TLC). After the completion of the reaction, the mixture was diluted in water and extracted with ethyl acetate (3 × 25 mL). The organic layer was separated and dried (Na_2SO_4). The crude product was obtained by removing the solvent *in vacuo* and was then purified by column chromatography using petroleum ether as the eluent to obtain *N*-propargyl-4-methoxyaniline **1**.

Synthesis of *N*-propargyl-6-methoxy-4-(2′-oxopyrrolidin-1′-yl)-1,2,3,4 tetrahydroquinoline 4

In a round bottom flask, a 5 mL solution in acetonitrile (MeCN) HPLC grade of preformed *N*-propargyl-4-methoxylaniline **1** (1 mmol) and formaldehyde **2** (1.1 mmol) were prepared and stirred for 10 min. Different Lewis acids (20 mol%) were added to the MeCN. After 20 min, a solution of *N*-vinyl-2-pyrrolidinone **3** (1.1 mmol) in MeCN was added to the reaction mixture and vigorously stirred. The resulting mixture was then stirred. After the reaction was achieved, as indicated by TLC, the reaction mixture was diluted with water (30 mL) and extracted with ethyl acetate (3 × 15 mL). The organic layer was separated and dried (Na_2SO_4). The crude product was obtained by solvent removal under vacuum, purified by column chromatography, and eluted with an appropriate mixture of petroleum ether and ethyl acetate to afford pure *N*-propargyl tetrahydroquinoline **4**.

Brown solid. m.p. 154–156 °C; IR (ATR): 3264, 2956, 2934, 2874, 2808, 1672, 1498, 1060, 803 cm^{-1}; ^1H NMR (400 MHz, $CDCl_3$): 1.92–2.04 (2H, m), 2.05–2.16 (2H, m), 2.14 (1H, t, J = 2.4 Hz), 2.46–2.50 (2H, m), 3.09–3.3 (2H, m), 3.18–3.35 (2H, m), 3.71 (3H, s, 6-OCH_3), 3.91 (1H, dd, J = 18.1, 2.4 Hz), 4.04 (1H, dd, J = 18.1, 2.4 Hz), 5.40 (1H, dd, J = 8.8, 6.4 Hz, 4-H), 6.51 (1H, d, J = 2.8 Hz), 6.72 (1H, d, J = 8.9 Hz), 6.77 (1H, ddd, J = 8.9, 2.8, 0.4 Hz); ^{13}C NMR (100 MHz, $CDCl_3$): 18.4, 26.9, 31.5, 41.4, 43.7, 47.8, 48.0, 55.7, 72.3, 79.2, 113.6, 114.0, 114.6, 122.9, 139.7, 152.5, 175.5; MS (ESI-IT), m/z: 307.1$[M + Na]^+$, 591.1$[2M + Na]^+$; Anal. Calcd for $C_{17}H_{20}N_2O_2$: C, 71.81; H, 7.09; N, 11.25%. Found: C, 71.72; H, 7.01; N, 11.06%. The NMR and ESI-MS data matched previously reported data.[22]

Computational methodology

All quantum calculations were performed using the GAUSSIAN 09 program suite.[28] The visualization of the analyzed structures was carried out through the VMD software.[29] The structure of the free reactants, transition state, intermediates, and free products were optimized using the density functional theory approach, with the Lee–Yang–Parr hybrid correlation–exchange functional B3LYP[30] together with the 6-31++G** basis set for all atoms except Bi and In, which were treated with relativistic effects with LanL2DZ core potentials.[31] In addition, dispersion corrections[32] (Grimme's D3BJ dispersion with Becke–Johnson damping) have been included in the DFT calculations. Frequency calculations were performed to determine the nature of all stationary points. That is, there are zero imaginary frequencies for the minimum and one imaginary frequency for the transition states. The corresponding transition state along the reaction coordinates for each stage was determined using Berny's analytical gradient optimization method, and was subsequently confirmed to be connected to the respective minima in the entrance channel of the pre-reactive and product complexes by performing scans using the intrinsic reaction coordinate (IRC) algorithm and setting a mass-weighted coordinate step size of 0.05 $amu^{1/2}$ Bohr.[33] The solvent effects of acetonitrile were mimicked with the implicit SMD continuum solvation model[34] by performing single-point energy calculations for the DFT-optimized geometry in vacuum. The free energy of the solution was calculated using the following equation.

$$\Delta G^0 = E_0^{DFT} + G_{corr}^{DFT} + \Delta G_{SMD}^{DFT} + \Delta G_{1atm\rightarrow 1M}$$

where E_0^{DFT} is the electronic energy calculated from DFT, G_{corr}^{DFT} is the thermal correction to Gibbs free energy under standard conditions (T = 298.15 K, pressure = 1 atm), ΔG_{SMD}^{DFT} is the solvation free energy, and $\Delta G_{1atm\rightarrow 1M}$ is an additional term for converting the 1 atm standard pressure in the gas phase to a standard concentration of 1 mol L^{-1} in the bulk phase with a value of 1.89 kcal mol^{-1}.[34] Electronic structure analysis of the stationary points involved in the intermediate iminium ion formation and cyclization processes was performed using the Multiwfn program.[35] The reactivity index, electronic populations, and noncovalent analysis were obtained using conceptual DFT,[36] electronic localization function (ELF) topology,[37] and NCI index,[38,39] respectively. In particular, the reactivity descriptors utilized included the chemical potential (μ),[40] global hardness (η),[41] global electrophilicity (ω),[42] and Parr function.[43]

Results and discussion

Synthesis of *N*-propargyl tetrahydroquinoline 4

The synthesis of the corresponding *N*-propargyl-6-methoxy-4-(2′-oxopyrrolidin-1′-yl)-1,2,3,4-THQ **4** was carried out using an

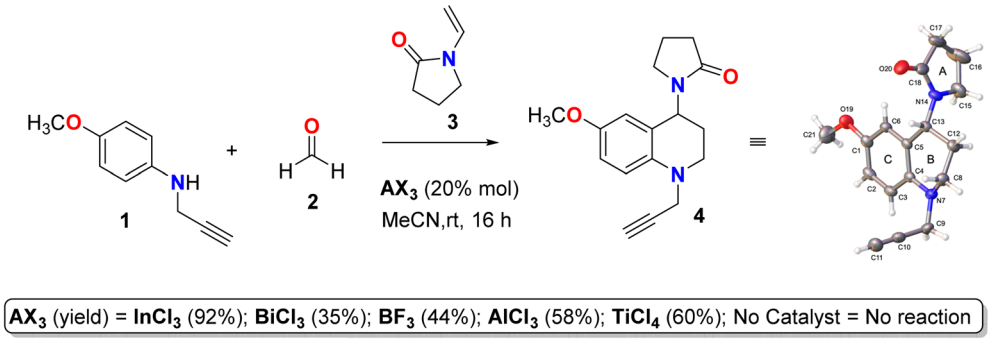

Scheme 1 Synthesis of *N*-propargyl 1,2,3,4-tetrahydroquinoline **4** *via* a one-pot three-component cationic Povarov reaction. ORTEP plot of THQ **4**. Thermal ellipsoids were drawn at a probability of 30%.

efficient methodology based on the acid-catalyzed one-pot three-component cationic Povarov reaction. *N*-propargyl THQ **4** was prepared in anhydrous MeCN (HPLC grade) at room temperature overnight between preformed *N*-propargyl-4-methoxyaniline **1**, formaldehyde **2**, and *N*-vinyl-2-pyrrolidinone **3**, according to our previously reported synthetic methodology.

To evaluate the effect of the different Lewis acids as catalysts, the reaction was performed in the absence and presence of the different Lewis catalysts, including $InCl_3$, $BiCl_3$, $AlCl_3$, $TiCl_4$ and $BF_3{\cdot}OEt_2$ (20 mol% stoichiometric ratio). As expected, no conversion was observed under the evaluated reaction conditions when no catalyst was used, and the precursor substrates remained unchanged in the reaction medium. The use of any of the Lewis catalysts evaluated led to reactions taking place in high and moderate yields. In the case of $InCl_3$, the highest yield was observed (92%), thus corroborating once again the remarkable catalytic effect of indium(III) salts in the conventional or cationic Povarov reaction (Scheme 1).

Molecular structure

Tetrahydroquinoline **4** crystallizes in a non-centrosymmetric monoclinic *Cc* space group with four entities per unit cell ($Z' = 1$). The molecule contains three rings, labeled A, B, and C (Fig. 1). Rings B (–C5–C4–N7–C8–C12–C13–) and C (–C5–C6–C1–C2–C3–C4–) were nearly coplanar, with a dihedral angle of 3.77(9)°. Ring A, which is bonded to atom C13, forms angles of 93.23(6)° with ring B and 93.06(16)° with ring C, indicating an almost orthogonal orientation between the rings. Furthermore, the torsion angle N14–C13–C5–C6 is −38.3(4)°, which is similar to the values reported for analog compounds.[44] In ring B, the puckering parameters[45] θ and φ were calculated to be 132.7(3)° and 89.3(4)°, respectively, suggesting a half-chair conformation for the six-membered ring. The average bonding distances for the *N*-propargyl fragment were within the expected ranges, according to previous reports,[44,46,47] with values of 1.460(4) Å for N7–C9, 1.477(5) Å C9–C10, and 1.175(5) Å for C10–C11. Table 1 summarizes the crystal data, data collection parameters, and refinements.

Computational details

For simplicity, we divide the analysis of the reaction mechanism into two parts. The first part shows the effects of the catalyst (Fig. 1), and the second part presents the relative Gibbs energies of the reaction steps (in the first stage). The Free Reactants (FR) are *N*-propargyl-4-methoxyaniline **1** + formaldehyde **2** + catalyst

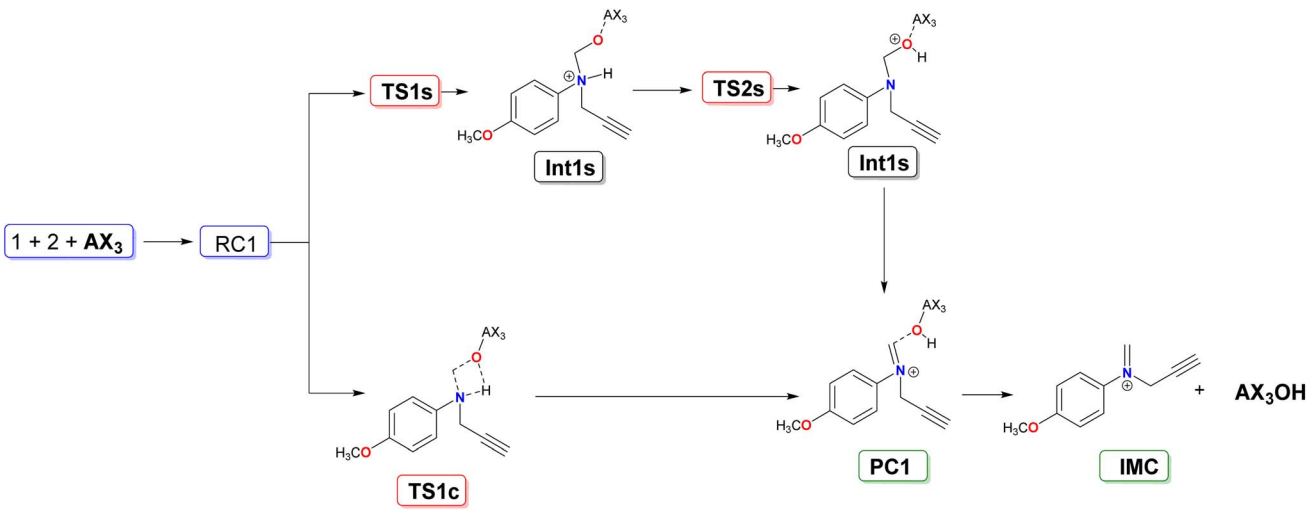

Fig. 1 Activation of formaldehyde and role of catalyst in formation of iminium ion (IMC).

Table 1 Crystal data and refinement details THQ **4**

Crystal data			
Empirical formula	$C_{17}H_{20}N_2O_2$	μ mm^{-1}	0.081
Formula weight	284.35	F(000)	608.0
Temperature/K	296.15	Crystal size/mm^3	0.226 × 0.182 × 0.052
Crystal system	Monoclinic	Radiation	MoKα ($\lambda = 0.71073$)
Space group	*Cc*	2Θ range for data collection/°	4.68 to 54.986
a [Å]	9.4298(3)	Index ranges	$-12 \le h \le 11$, $-22 \le k \le 22$, $-12 \le l \le 12$
b [Å]	17.4070(7)	Reflections collected	17 238
c [Å]	9.4334(4)	Independent reflections	3314 [$R_{int} = 0.0455$, $R_{sigma} = 0.0329$]
α [°]	90	Data/restraints/parameters	3314/2/191
β [°]	96.2680(10)	Goodness-of-fit on F^2	1.055
γ [°]	90	Final R indexes [$I \ge 2\sigma(I)$]	$R_1 = 0.0440$, w$R_2 = 0.1138$
Volume [Å^3]	1539.18(10)	Final R indexes [all data]	$R_1 = 0.0546$, w$R_2 = 0.1212$
Z	4	Largest diff. peak/hole/e Å^{-3}	0.13/−0.20
ρ_{calc} g cm^{-3}	1.227	CCDC number	2 415 596

($InCl_3$, $BiCl_3$ or BF_3), the complex between FR and the catalyst (RC1), and the Free Products (FP) are the iminium ion + AX_3OH ($InCl_3OH$, $BiCl_3OH$ or BF_3OH). The rest of the intermediates and transition states are shown in Fig. 1.

It is remarkable to note that in the reactivity study, all catalysts experimentally tested were considered. However, for the reaction mechanism analysis, only three catalysts were selected, in the following order: $InCl_3$, which demonstrated the highest yield; $BiCl_3$, which displayed an intermediate yield; and BF_3, which yielded the least.

Effect of the catalyst. By considering the interaction between the catalyst and the free reactants, the stabilization energy can

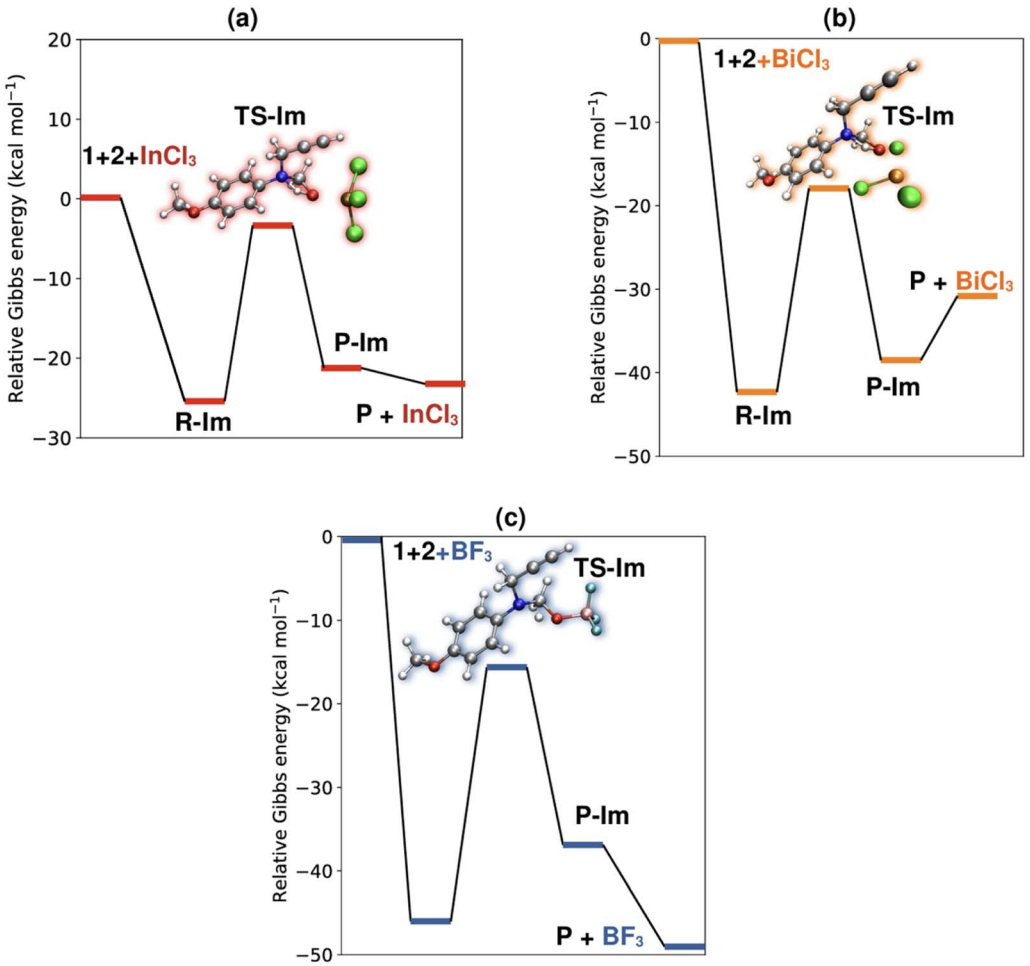

Fig. 2 Free Gibbs energy (kcal mol^{-1}) for catalyzed formation of iminium ion intermediates using (a) $InCl_3$, (b) $BiCl_3$, and (c) BF_3. Carbon (gray), hydrogen (white), nitrogen (blue), oxygen (red), chlorine (green), fluorine (cyan), indium (brown), bismuth (gold), boron (pink).

be associated with the O–AX_3 interaction (Fig. 2) For $InCl_3$ and BF_3 the stabilization energies are 12.0 and 37.0 kcal mol^{-1}, respectively, which suggests that both O–$InCl_3$ and O–BF_3 bonding interactions are favored.

However, for the $BiCl_3$ catalyst, the formation of RC1 involved a small barrier of 5.0 kcal mol^{-1}. Interestingly, based on our experimental studies, the smallest yields were obtained with the $BiCl_3$ catalyst. It also shows that the catalyst with the lowest Free Energy barrier is $InCl_3$, which is approximately 23.2 kcal mol^{-1}, which agrees with the experimental results because BF_3 and $BiCl_3$ exhibit higher energy barriers of 26.9 and 24.1 kcal mol^{-1}, respectively.

An energy barrier is also obtained without the catalyst. In this case, by optimizing the geometry of the RC1 structure, which is a reaction intermediate just before the transition state, a geometry is obtained in which the aldehyde is rejected by the reactant (the most stable C–N distance is approximately 2.82 Å). Considering the configuration of this intermediate, it seems improbable that a transition state can be reached. This justifies the experimental result obtained without the catalyst, where the proposed reaction did not give any yield. In the Povarov reaction, a cationic 2-azadiene system was generated *in situ* by reacting N-substituted aniline with the corresponding aldehyde. Cationic species are sufficiently electrophilic and can undergo nucleophilic attack from electron-rich olefins to yield the desired tetrahydroquinoline. The acid catalyst is involved in aldehyde activation that generates an attack of the N-substituted amine, generating the iminium ion; consequently, the reactivity of the aldehyde-catalyst complex could play a crucial role in the global cationic Povarov occurrence. Five Lewis acids ($InCl_3$, $BiCl_3$, $AlCl_3$, $TiCl_4$ and BF_3) were experimentally evaluated for their ability to facilitate the formation of compound **4**. Among these, $InCl_3$ exhibited the highest reaction performance (Scheme 1). Theoretical analysis of the catalyst was performed by calculating the global and local reactivity indices using a conceptual DFT framework (CDFT). Table 2 shows several of the global reactivity indices mostly used in CDFT, the chemical potential (μ) values show that the effect of the catalyst makes the formaldehyde more electronegative, especially for BF_3.

Considering the global reactivity indexes, upon O–cat coordination, formaldehyde's chemical potential (μ) becomes more negative, indicating greater electron-accepting ability, with the largest shifts observed for BF_3 and $TiCl_4$ ($\mu \approx -0.248$ and -0.244) and the smallest for $BiCl_3$ ($\mu = -0.211$). Chemical hardness (η) decreases in all cases, with $BiCl_3$ yielding the lowest hardness ($\eta = 0.303$), enhancing reactivity. $TiCl_4$ facilitates the highest electron transfer ($\Delta N_{max} = 0.817$), while $BiCl_3$ shows the lowest ($\Delta N_{max} = 0.697$). In terms of global electrophilicity (ω), $TiCl_4$ stands out ($\omega = 2.713$), followed by BF_3 (1.910) and $BiCl_3$ (2.000). Overall, $TiCl_4$ and BF_3 are more effective at activating and stabilizing formaldehyde, whereas $BiCl_3$ exhibits weaker catalytic effects.

In the context of local reactivity, the condensed Parr (P_k^-, P_k^+) functions and the local electrophilicity index have been used (ω_k). Table 3 shows the condensed spin densities for the radical anion and radical cation (atom-condensed Parr functions) for formaldehyde and its catalyzed form.

In addition, the results show a clear correlation between the global electrophilicity index (ω_k) of the catalysts and their respective reaction yields. In general, catalysts with higher ω_k values tend to produce higher yields, suggesting that the catalyst's ability to accept electron density plays a key role in its efficiency. $InCl_3$, with the highest ω_k value (1.161), achieves the highest yield (92%), indicating strong stabilization of the transition state and enhanced activation of formaldehyde. BF_3, with an intermediate ω_k value (1.061), also shows a relatively high yield (44%), while $TiCl_4$ and $AlCl_3$, with lower ω_k values (0.778 and 0.604, respectively), exhibit moderate yields (60% and 58%). $BiCl_3$, despite having a lower ω_k value than BF_3 and $InCl_3$ (0.700), results in a lower yield (35%), suggesting that additional factors beyond ω_k may influence its catalytic performance. Overall, these findings reinforce the idea that the electronic activation of formaldehyde by the catalyst, as evidenced by

Table 2 Global parameters calculated for formaldehyde without and with the five catalysts studied

	CH_2O	$CH_2O\cdots BF_3$	$CH_2O\cdots BiCl_3$	$CH_2O\cdots InCl_3$	$CH_2O\cdots AlCl_3$	$CH_2O\cdots TiCl_4$
μ	−0.186	−0.248	−0.211	−0.221	−0.225	−0.244
η	0.429	0.437	0.303	0.339	0.326	0.299
ΔN^{max}	0.434	0.567	0.697	0.651	0.691	0.817
ω	1.102	1.910	2.000	1.957	2.117	2.713

Table 3 Condensed Parr functions: condensed spin densities for the radical anion and radical cation for formaldehyde and its catalyzed form

	CH_2O		$CH_2O\cdots BF_3$		$CH_2O\cdots BiCl_3$		$CH_2O\cdots InCl_3$		$CH_2O\cdots AlCl_3$		$CH_2O\cdots TiCl_4$	
	P_k^-	P_k^+	P_k^-	P_k^+	P_k^-	P_k^+	P_k^-	P_k^+	P_k^-	P_k^+	P_k^-	P_k^+
C	0.439	0.062	0.555	0.150	0.350	0.158	0.593	0.135	0.494	0.066	0.489	0.062
O	0.288	0.751	0.258	0.614	0.603	0.622	0.291	0.647	0.278	0.760	0.304	0.759
H	0.135	0.093	0.092	0.109	0.023	0.112	0.058	0.110	0.091	0.088	0.104	0.089
H	0.135	0.093	0.094	0.126	0.024	0.109	0.058	0.108	0.138	0.086	0.103	0.090

Table 4 Electrophilicity index ω_k (eV) for formaldehyde carbon, both isolated and with study catalysts, including reaction yields[a]

Catalyst	Yields[b] (%)	ω_k
No catalyst	ND	0.484
$BiCl_3$	35	0.700
BF_3	44	1.061
$InCl_3$	92	1.161
$AlCl_3$	58	0.604
$TiCl_4$	60	0.778

[a] ND: not determined. [b] Isolated yield after column chromatography.

variations in its local electronic properties, is directly related to reaction efficiency, with $InCl_3$ being the most effective and $BiCl_3$ the least favorable catalyst. Note that when observing the yield values and electrophilicity index, this leads us to believe that the effect of the catalyst increases the electrophilic character of the formaldehyde carbon, favoring the reaction with *N*-propargylaniline **1** and the formation of product **4** (Scheme 1) (Table 4).

Chemical bond analysis in the cationic Povarov reaction mechanism. A crucial concept for describing chemical reactions is bond formation/breaking analysis. It is essential to remember that the electronic structure of the transition states (TS) provides key elements for revealing information about reactivity. In the cationic Povarov reaction context, we decided to analyze the chemical bonding in the three TS associated with iminium cation formation using the previously mentioned catalysts. For this purpose, we employed the electron localization function (ELF), which was calculated primarily over the N–H–O–CH_2 reaction center. ELF is closely related to the Lewis model representation, allowing us to estimate the average number of electrons associated with shells, lone pairs, and bonds. Fig. 3 shows the number of electrons in the N(X–Y) bonds and N(X) lone pairs involved in Stage 1 of the cationic Povarov reaction. It should be noted that TS involves the formation of an N–C bond between *N*-propargylaniline **1** and the carbon of the formaldehyde-catalyst complex, as evidenced by $N(X) = 1.8e$. Furthermore, it is important to mention that the N–H bond had not yet been completely broken, with a value of $N(N–C) = 1.9e$. These observations were consistent across all the analyzed catalysts.

Interestingly, there were differences in the formation of O–H bonds among the three catalysts. For example, for $InCl_3$ and $BiCl_3$, the number of electrons in O–H is close to $1.0e$, whereas for BF_3, this value is $1.8e$. However, the valence shell of the oxygen atom in the case of $BiCl_3$ presents two lone pairs (N(O1) and N(O2)) instead of one (N(O1)), as observed for both $InCl_3$ and BF_3.

In connection with the thermodynamic analysis discussed earlier, the accumulation of pair density on the O–H bond and the valence shell of oxygen could increase the barrier height during the formation of the iminium cation. This effect was more pronounced in the $BiCl_3$-catalyzed system. Likewise, the structural analysis of the transition states (TS) associated with the formation of the iminium cation reveals significant differences in bond distances depending on the nature of the catalyst, as shown in Table 5. The interaction between the catalyst and the oxygen atom of formaldehyde (Cat–O) is notably stronger for BF_3 (1.58 Å) compared to $BiCl_3$ (2.16 Å) and $InCl_3$ (2.08 Å), suggesting a greater Lewis acidity and a stronger polarization of the carbonyl group. However, despite this stronger interaction, the reaction yield follows the trend: $InCl_3$ (92%) ≫ BF_3 (44%) > $BiCl_3$ (35%), indicating that factors beyond the strength of the catalyst–substrate interaction play a critical role in determining catalytic efficiency.

The C–O bond distances remain relatively consistent across all three catalysts (1.42–1.44 Å), indicating a similar degree of

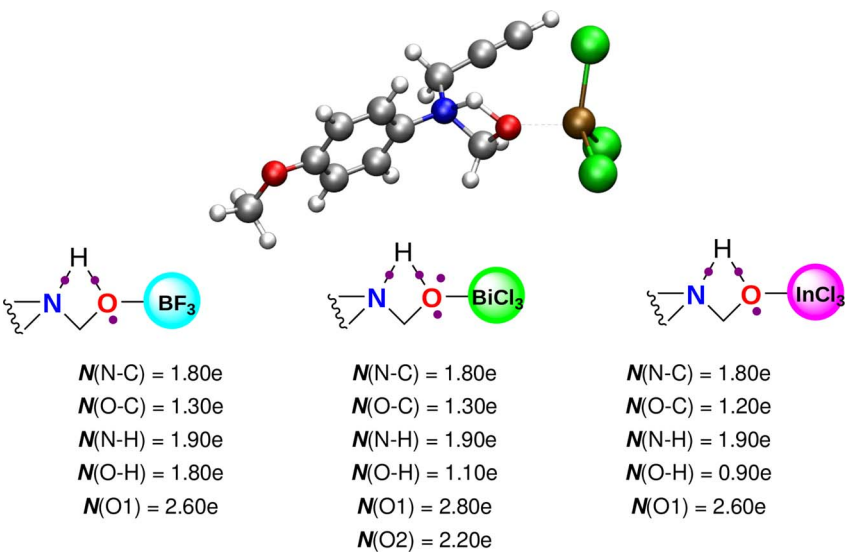

Fig. 3 Lewis structures determined through ELF topological analysis of the transition states associated with the iminium cation generation stage using BF_3, $BiCl_3$ and $InCl_3$. The electronic populations of N(X–Y) and N(X) lone pairs are also shown. In addition, the structure of the transition state associated with the $InCl_3$-catalyzed system is shown.

Table 5 Bond distances in the transition states of iminium cation formation using BF_3, $BiCl_3$ and $InCl_3$ as catalysts

	BF_3	$BiCl_3$	$InCl_3$
Cat–O	1.58	2.16	2.08
C–O	1.42	1.44	1.42
N–C	1.51	1.50	1.51
O–H	1.27	1.24	1.26
N–H	1.29	1.32	1.30

carbonyl activation. Likewise, the N–C bond, characteristic of iminium formation, is nearly invariant (1.50–1.51 Å), suggesting that the transition state structure is maintained regardless of the catalyst. However, subtle variations in O–H and N–H distances suggest differences in proton transfer reaction, which may impact reaction rates and product stabilization. The remarkable yield observed for $InCl_3$ (92%), despite its weaker Cat–O interaction, suggests that additional catalytic factors—such as electronic effects, solvation, or secondary interactions—play a key role in facilitating iminium ion formation. In contrast, although $BiCl_3$ exhibits the shortest Cat–O bond, its moderate yield (44%) suggests that an overly strong interaction may hinder turnover or lead to catalyst deactivation.

In the second stage, two possible cyclization pathways were proposed: concerted and stepwise process (Fig. 4). Following these reaction routes, the potential product formed by the stepwise pathway yields only product **4** (**P-Cs**), while the concerted pathway (**P-Cc**) yields THQ **4** and their possible regioisomer THQ **5**. However, our experimental results indicate the exclusive formation of compound **4**, suggesting that **P-Cs** are preferred. This finding is further supported by the energy profile and no covalent interaction analysis described later, which reinforces the feasibility of a stepwise mechanism.

Fig. 5 depicts the energy barriers (kcal mol^{-1}) of concerted and stepwise cyclizations. In general, the concerted *via* involves only a transition state (**TS-Cc**) with a barrier of 28 kcal mol^{-1}, in contrast, stepwise cyclization involves two transition states: **TS1-Cs** and **TS2-Cs.** The first stage involves the formation of intermediate **Int-Cs** (Mannich adduct), where the C–C bond forms between the olefinic carbon of **IMC** and another olefinic carbon belonging to **3**, which involves a barrier of ~6 kcal mol^{-1}.

In addition, **P-Cs** formation (the final product of cyclization) entails **TS2-Cs** starting from **Int-Cs** with a low barrier of ~1 kcal mol^{-1}. In this context, a comparison of the energy profiles in Fig. 5 indicates that stepwise cyclization is favored over concerted cyclization, which occurs through intramolecular Friedel–Crafts alkylation reaction (Fig. 6).

Table 6 reports the geometrical data concerning the transition states involved in the conversion of *N*-vinyl-2-pyrrolidinone and the iminium cation into *N*-propargyl-6-methoxy-4-(2′-oxopyrrolidin-1′-yl)-1,2,3,4-tetrahydroquinoline. The bond distances in the concerted transition state (**TS-Cc**) indicate a synchronous bond reorganization. The C1–C2 (1.41 Å) and C3–C4 (1.43 Å) bond lengths are close to typical single/double bond values, while the C2–C3 bond remains elongated at 2.44 Å, suggesting significant electronic reorganization.

The N–C5 (1.37 Å) and C1–C5 (1.87 Å) distances indicate the formation of the tetrahydroquinoline ring in a single step. On the contrary, considering the stepwise pathway in **TS1-Cs**, the formation of key bonds is less advanced, as indicated by the significantly elongated C2–C3 (3.76 Å) and C3–C4 (3.21 Å) distances. The C1–C5 bond (2.24 Å) is also longer than in **TS-Cc**, suggesting an initial stage of bond rearrangement. The N–C5 distance (1.33 Å) is slightly shorter than in **TS-Cc**, possibly due to stronger stabilization of the iminium moiety at this stage. In addition, **TS2-Cs** represents the second step of the reaction, where bond formation is more advanced. The C2–C3 distance contracts significantly (2.11 Å), indicating partial bond formation, while the C1–C5 bond (1.56 Å) shortens compared to **TS1-Cs** but remains longer than in **TS-Cc**, suggesting that the final structural reorganization is still incomplete. The N–C5 bond elongates to 1.44 Å, reflecting the final electronic adjustments needed to achieve the product structure.

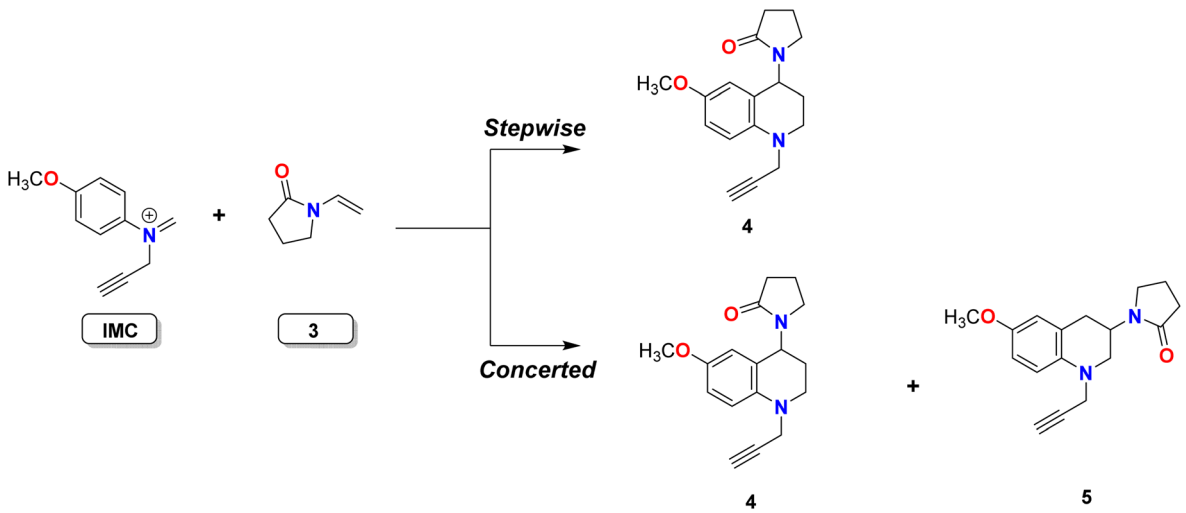

Fig. 4 Overall reaction to obtain (3-yl, 4-yl) THQs from their corresponding IMC and *N*-vinyl-2 pyrrolidinone (3).

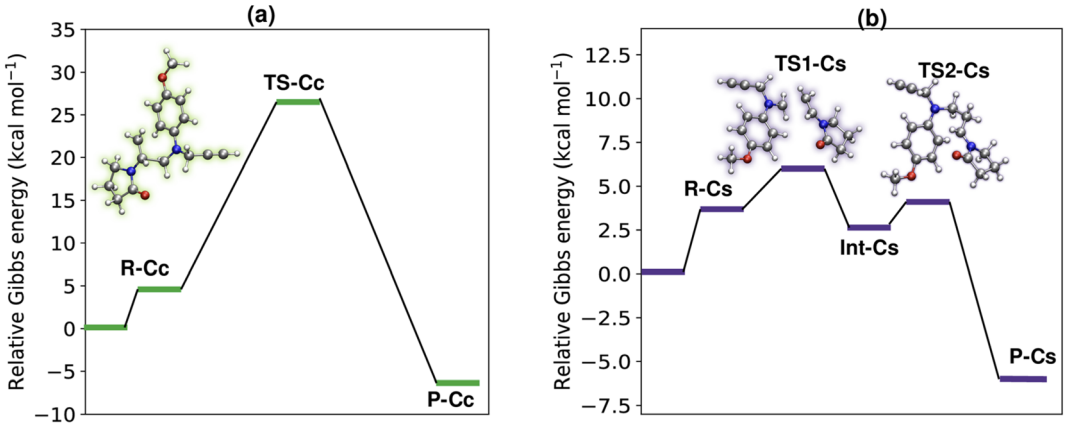

Fig. 5 Free energy kcal mol^{-1} for the concerted (panel a) and stepwise (panel b) cyclization stages of the IMC + 3 reaction.

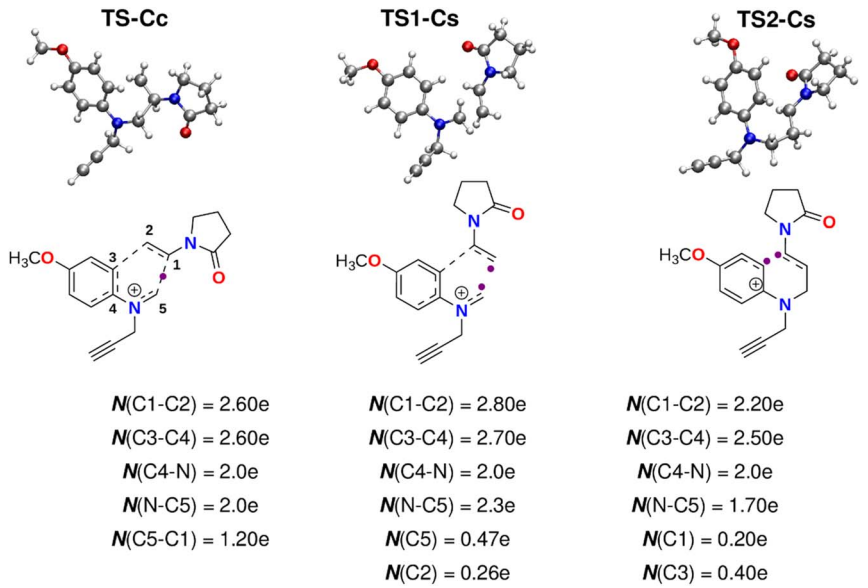

Fig. 6 Lewis structures determined through ELF topological analysis of the transition states associated with the concerted (TS-Cc) and stepwise (TS1-Cs, TS2-Cs) cyclization IMC + 3. The electronic populations of the N(X–Y) bonds and N(X) lone pairs are also shown. Additionally, the structures of the transition states for concerted (TS-Cc) and stepwise (TS1-Cs, TS2-Cs) cyclizations are depicted.

Table 6 Bond distances in the transition states (TSc, TSc1, and TSc2) for the formation of *N*-propargyl-6-methoxy-4-(2′-oxopyrrolidin-1′-yl)-1,2,3,4-tetrahydroquinoline from *N*-vinyl-2-pyrrolidinone and the iminium cation

	C1–C2	C2–C3	C3–C4	C4–N	N–C5	C1–C5
TS-Cc	1.41	2.44	1.43	1.38	1.37	1.87
TS1-Cs	1.38	3.76	3.21	1.43	1.33	2.24
TS2-Cs	1.51	2.11	1.44	1.36	1.44	1.56

Chemical bonding analysis of the cyclization stage reveals bonding patterns that differentiate the concerted route from the stepwise one. In the concerted route, the formation of the first C–C bond was observed with an electron number of N(C5–C1) = 1.2e. This electron population, which is less than 2.0e, corresponds to a highly delocalized single bond formed in **TS-Cc**. Additionally, the double bond C1=C2 in **3** was significantly weakened with N(C1–C2) = 2.6e.

Considering the stepwise route, in **TS1-Cs**, the first C–C bond has not yet formed, as there are non-bonding electron density centers on the C2 and C5 carbons. That is, the electron density was not shared between the carbons of **IMC** (C5) and **3** (C2), with electron populations of N(C5) = 0.47e and N(C2) = 0.26e. Subsequently, after **IntS** formation in **TS2-Cs**, the C2–C5 bond emerges with N(C2–C5) = 1.8e. However, the remaining C–C bond for **P-Cs** formation has not yet emerged in **TS2-Cs**, as the pairing density is divided between the C1 and C3 carbons N(C1) = 0.20e and N(C3) = 0.46e. In summary, the high energy barrier of the concerted process could be attributed to the presence of bonding density, which characterizes the formation of the first C–C bond between **IMC** and **3**. In contrast, for the stepwise

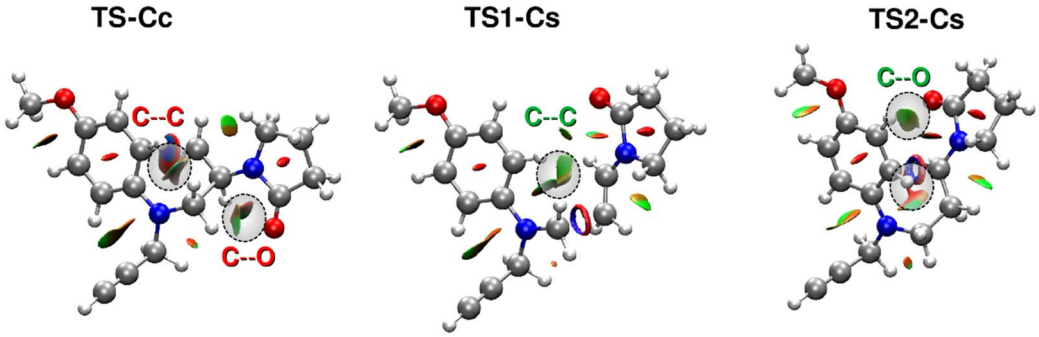

Fig. 7 Non-covalent interaction analysis of **TS-Cc**, **TS1-Cs**, and **TS2-Cs** structures using a reduced density gradient isosurface of 0.5.

process, C–C bond formation is preceded by the appearance of non-bonding density centers, associated with relatively low energy barriers.

In addition, we performed noncovalent interaction calculations using a reduced-gradient density scalar field. The results for the **TS-Cc**, **TS1-Cs**, and **TS2-Cs** structures are shown in Fig. 7. Notably, in the **TS-Cc** structure, there are repulsive C–C and C–O interactions. Specifically, C–C repulsion arises between the six-membered ring of *N*-propargyl-4-methoxyanilinium and the *N*-vinyl-2-pyrrolidinone moiety. Similarly, a C–O repulsive interaction occurred between the carbonyl group of *N*-vinyl-2-pyrrolidinone and the CH_2–CH fragment present in both reactants. Interestingly, these interactions exhibit different characteristics in stepwise transition states (**TS1-Cs** and **TS2-Cs**), where van der Waals interactions replace the repulsive force observed in the concerted mechanism. This is particularly relevant because the high barrier associated with the concerted mechanism correlates with repulsive interactions during cyclization. Conversely, the lower barriers of the stepwise mechanism are linked to van der Waals interactions, which mitigate the repulsive interactions characteristic of the cyclization process.

Conclusions

Theoretical analysis using DFT and ELF demonstrated that $InCl_3$ is the most efficient catalyst for the cationic Povarov reaction, providing the lowest Gibbs free energy barrier and highest reaction yield.

Our findings reveal that the interaction between the catalyst and reactants significantly enhances the reactivity of the aldehyde, facilitating the formation of the iminium ion intermediate and subsequent cyclization to yield the desired tetrahydroquinoline product. The analysis of the global and local reactivity indices further supports the conclusion that the catalyst increases the electrophilic character of the formaldehyde carbon, promoting the reaction. Additionally, the chemical bonding analysis of the iminium cation formation suggests that the high accumulation of pairing density over the O–H bond increases the reaction barrier.

For the cyclization stage, our results indicate that concerted cyclization involves C–C bond formation in the transition state, implying a high energy barrier. In contrast, the stepwise pathway shows that both C–C bonds emerge from non-bonding centers originating in the two transition states, each with low-energy barriers. This energetically favorable route, which leads to obtaining the final product THQ, involves the formation of a Mannich-adduct and finally a cyclization reaction *via* Friedel–Crafts intramolecular alkylation.

Based on these results, we propose that the term 'Diels–Alder' should no longer be used to describe these types of reactions. This study provides a detailed understanding of the mechanism of the cationic Povarov reaction and the influence of Lewis acid catalysts, which can be leveraged to optimize and develop new synthetic strategies for tetrahydroquinoline derivatives with potential pharmacological applications.

Data availability

Main data or spectra utilized and analyzed in this study are available or described in the manuscript. No datasets were generated during this study. And data supporting this article has been included as part of the ESI.†

Conflicts of interest

The authors declare no conflicts of interest.

Acknowledgements

The authors would like to thank the Vicerectoria de Investigaciones y extensión of the Universidad Industrial de Santander, Colombia, for financial support for part of this research (project code 3737). Acknowledgments to Fondequip EQM 200138. E. P.-C. thanks FONDECYT Post-Doctoral Fellowship No. 3220681. Y. A. R.-N thanks UNAB for financial support (project Dl-05.23/REG).

References

1 N. Kerru, L. Gummidi, S. Maddila, K. K. Gangu and S. B. Jonnalagadda, A Review on Recent Advances in Nitrogen-Containing Molecules and Their Biological Applications, *Molecules*, 2020, **25**, 1909, DOI: 10.3390/molecules25081909.

2 J. N. Hanna, F. Ntie-Kang, M. Kaiser, R. Brun and S. M. N. Efange, 1-Aryl-1,2,3,4-tetrahydroisoquinolines as potential antimalarials: synthesis, *in vitro* antiplasmodial activity and *in silico* pharmacokinetics evaluation, *RSC Adv.*, 2014, **4**, 22856–22865, DOI: **10.1039/C3RA46791K**.

3 S. Farooq, A. Mazhar, A. Ghouri, I. Ul-Haq and N. Ullah, One-Pot Multicomponent Synthesis and Bioevaluation of Tetrahydroquinoline Derivatives as Potential Antioxidants, α-Amylase Enzyme Inhibitors, Anti-Cancerous and Anti-Inflammatory Agents, *Molecules*, 2020, **25**, 2710, DOI: **10.3390/molecules25112710**.

4 M. Gutiérrez, U. Carmona, G. Vallejos and L. Astudillo, Antifungal Activity of Tetrahydroquinolines against Some Phytopathogenic Fungi, *Z. fur Naturforsch. C*, 2012, **67**, 551–556, DOI: **10.1515/znc-2012-11-1204**.

5 A. M. Alafeefy, Design, synthesis, and antitumor screening of certain novel tetrahydroquinoline sulfonamides, *J. Enzyme Inhib. Med. Chem.*, 2015, **30**, 189–194, DOI: **10.3109/14756366.2014.899595**.

6 H. M. F. Madkour, M. A. E. M. El-Hashash, M. S. Salem, A. O. A. Mahmoud and Y. M. S. A. Al kahraman, Design, Synthesis, and *In Vitro* Antileishmanial and Antitumor Activities of New Tetrahydroquinolines, *J. Heterocycl. Chem.*, 2018, **55**, 391–401, DOI: **10.1002/jhet.3046**.

7 I. Muthukrishnan, V. Sridharan and J. C. Menéndez, Progress in the Chemistry of Tetrahydroquinolines, *Chem. Rev.*, 2019, **119**, 5057–5191, DOI: **10.1021/acs.chemrev.8b00567**.

8 Y. Ren, Y. Wang, X. Li, Z. Zhang and Q. Chi, Selective hydrogenation of quinolines into 1,2,3,4-tetrahydroquinolines over a nitrogen-doped carbon-supported Pd catalyst, *New J. Chem.*, 2018, **42**, 16694–16702, DOI: **10.1039/C8NJ04014A**.

9 A. Palanimuthu, C. Chen and G.-H. Lee, Synthesis of highly substituted tetrahydroquinolines using ethyl cyanoacetate *via* aza-Michael–Michael addition, *RSC Adv.*, 2020, **10**, 13591–13600, DOI: **10.1039/D0RA01264E**.

10 D. S. Giera and C. Schneider, InCl 3 -Catalyzed Allylic Friedel–Crafts Reactions toward the Stereocontrolled Synthesis of 1,2,3,4-Tetrahydroquinolines, *Org. Lett.*, 2010, **12**, 4884–4887, DOI: **10.1021/ol102023z**.

11 X.-P. Ma, K. Li, S.-Y. Wu, C. Liang, G.-F. Su and D.-L. Mo, Construction of 2,3-quaternary fused indolines from alkynyl tethered oximes and diaryliodonium salts through a cascade strategy of N -arylation/cycloaddition/[3,3]-rearrangement, *Green Chem.*, 2017, **19**, 5761–5766, DOI: **10.1039/C7GC02844J**.

12 J. S. Bello Forero, J. Jones Junior and F. M. da Silva, The Povarov Reaction as a Versatile Strategy for the Preparation of 1, 2, 3, 4-Tetrahydroquinoline Derivatives: An Overview, *Curr. Org. Synth.*, 2015, **13**, 157–175, DOI: **10.2174/1570179412666150706183906**.

13 J.-X. Huang, K.-Q. Hou, Q.-L. Hu, X.-P. Chen, J. Li, A. S. C. Chan and X.-F. Xiong, Organocatalytic Asymmetric Three-Component Povarov Reactions of Anilines and Aldehydes, *Org. Lett.*, 2020, **22**, 1858–1862, DOI: **10.1021/acs.orglett.0c00206**.

14 F. Palacios, C. Alonso, A. Arrieta, F. P. Cossío, J. M. Ezpeleta, M. Fuertes and G. Rubiales, Lewis Acid Activated Aza-Diels–Alder Reaction of N -(3-Pyridyl)aldimines: An Experimental and Computational Study, *Eur. J. Org. Chem.*, 2010, 2091–2099, DOI: **10.1002/ejoc.200901325**.

15 L. R. Domingo, M. J. Aurell, J. A. Sáez and S. M. Mekelleche, Understanding the mechanism of the Povarov reaction. A DFT study, *RSC Adv.*, 2014, **4**, 25268, DOI: **10.1039/c4ra02916j**.

16 L. R. Domingo, M. J. Aurell and P. Pérez, The mechanism of ionic Diels–Alder reactions. A DFT study of the oxa-Povarov reaction, *RSC Adv.*, 2014, **4**, 16567–16577, DOI: **10.1039/C3RA47805J**.

17 L. R. Domingo, M. Ríos-Gutiérrez and S. Emamian, Understanding the stereoselectivity in Brønsted acid catalysed Povarov reactions generating cis/trans CF 3 -substituted tetrahydroquinolines: a DFT study, *RSC Adv.*, 2016, **6**, 17064–17073, DOI: **10.1039/C5RA27650K**.

18 V. V. Kouznetsov, Recent synthetic developments in a powerful imino Diels–Alder reaction (Povarov reaction): application to the synthesis of N-polyheterocycles and related alkaloids, *Tetrahedron*, 2009, **65**, 2721–2750, DOI: **10.1016/j.tet.2008.12.059**.

19 R. Abonia, J. Castillo, B. Insuasty, J. Quiroga, M. Nogueras and J. Cobo, Efficient Catalyst-Free Four-Component Synthesis of Novel γ-Aminoethers Mediated by a Mannich Type Reaction, *ACS Comb. Sci.*, 2013, **15**, 2–9, DOI: **10.1021/co300105t**.

20 M. Acelas, A. Bohórquez and V. Kouznetsov, Highly Diastereoselective Synthesis of New trans-Fused Octahydro-acridines *via* Intramolecular Cationic Imino Diels–Alder Reaction of N-Protected Anilines and Citronellal or Citronella Essential Oil, *Synthesis*, 2017, **49**, 2153–2162, DOI: **10.1055/s-0036-1588713**.

21 R. R. R. Taylor and R. A. Batey, A Hetero Diels–Alder Approach to the Synthesis of Chromans (3,4-Dihydrobenzopyrans) Using Oxonium Ion Chemistry: The Oxa-Povarov Reaction, *J. Org. Chem.*, 2013, **78**, 1404–1420, DOI: **10.1021/jo302328s**.

22 Y. A. Rodríguez, M. Gutiérrez, D. Ramírez, J. Alzate-Morales, C. C. Bernal, F. M. Güiza and A. R. Romero Bohórquez, Novel N -allyl/propargyl tetrahydroquinolines: Synthesis *via* Three-component Cationic Imino Diels–Alder Reaction, Binding Prediction, and Evaluation as Cholinesterase Inhibitors, *Chem. Biol. Drug Des.*, 2016, **88**, 498–510, DOI: **10.1111/cbdd.12773**.

23 A. R. R. Bohórquez, J. Romero-Daza and M. Acelas, Versatile and mild HCl-catalyzed cationic imino Diels-Alder reaction for the synthesis of new tetrahydroquinoline derivatives, *Synth. Commun.*, 2016, **46**, 338–347, DOI: **10.1080/00397911.2015.1136646**.

24 G. M. Sheldrick, *SADABS, Software for Empirical Absorption Correction*, University of Göttingen, Göttingen, 2000.

25 G. M. Sheldrick, SHELXT – Integrated space-group and crystal-structure determination, *Acta Crystallogr., Sect. A: Found. Adv.*, 2015, **71**, 3–8, DOI: **10.1107/S2053273314026370**.

26 G. M. Sheldrick, Crystal structure refinement with SHELXL, *Acta Crystallogr., Sect. C: Struct. Chem.*, 2015, **71**, 3–8, DOI: 10.1107/S2053229614024218.

27 O. V Dolomanov, L. J. Bourhis, R. J. Gildea, J. A. K. Howard and H. Puschmann, OLEX2 : a complete structure solution, refinement and analysis program, *J. Appl. Crystallogr.*, 2009, **42**, 339–341, DOI: 10.1107/S0021889808042726.

28 M. Frisch, G. Trucks, H. Schlegel, G. Scuseria, M. Robb, J. Cheeseman, J. Montgomery, T. Vreven, K. Kudin, J. Burant, J. Millam, S. Iyengar, J. Tomasi, V. Barone, B. Mennucci, M. Cossi, G. Scalmani, N. Rega, G. Petersson, H. Nakatsuji, M. Hada, M. Ehara, K. Toyota, R. Fukuda, J. Hasegawa, M. Ishida, T. Nakajima, Y. Honda, O. Kitao, H. Nakai, M. Klene, X. Li, J. Knox, H. Hratchian, J. Cross, V. Bakken, C. Adamo, J. Jaramillo, R. Gomperts, R. Stratmann, O. Yazyev, A. Austin, R. Cammi, C. Pomelli, J. Ochterski, P. Ayala, K. Morokuma, G. Voth, P. Salvador, J. Dannenberg, V. Zakrzewski, S. Dapprich, A. Daniels, M. Strain, O. Farkas, D. Malick, A. Rabuck, K. Raghavachari, J. Foresman, J. Ortiz, Q. Cui, A. Baboul, S. Clifford, J. Cioslowski, B. Stefanov, G. Liu, A. Liashenko, P. Piskorz, I. Komaromi, R. Martin, D. Fox, T. Keith, A. Laham, C. Peng, A. Nanayakkara, M. Challacombe, P. Gill, B. Johnson, W. Chen, M. Wong, C. Gonzalez, J. Pople, *Gaussian 09, Revision D.01*, Gaussian, Inc., Wallingford CT, 2009.

29 W. Humphrey, A. Dalke and K. Schulten, VMD: visual molecular dynamics, *J. Mol. Graphics*, 1996, **14**, 33–38, DOI: 10.1016/0263-7855(96)00018-5.

30 A. D. Becke, Density-functional thermochemistry. III. The role of exact exchange, *J. Chem. Phys.*, 1993, **98**, 5648–5652, DOI: 10.1063/1.464913.

31 H. B. Schlegel, Optimization of equilibrium geometries and transition structures, *J. Comput. Chem.*, 1982, **3**, 214–218, DOI: 10.1002/jcc.540030212.

32 S. Grimme, S. Ehrlich and L. Goerigk, Effect of the damping function in dispersion corrected density functional theory, *J. Comput. Chem.*, 2011, **32**, 1456–1465, DOI: 10.1002/jcc.21759.

33 C. Gonzalez and H. B. Schlegel, Reaction path following in mass-weighted internal coordinates, *J. Phys. Chem.*, 1990, **94**, 5523–5527, DOI: 10.1021/j100377a021.

34 A. V. Marenich, C. J. Cramer and D. G. Truhlar, Universal Solvation Model Based on Solute Electron Density and on a Continuum Model of the Solvent Defined by the Bulk Dielectric Constant and Atomic Surface Tensions, *J. Phys. Chem. B*, 2009, **113**, 6378–6396, DOI: 10.1021/jp810292n.

35 T. Lu and F. Chen, Multiwfn: A multifunctional wavefunction analyzer, *J. Comput. Chem.*, 2012, **33**, 580–592, DOI: 10.1002/jcc.22885.

36 P. Geerlings, F. De Proft and W. Langenaeker, Conceptual Density Functional Theory, *Chem. Rev.*, 2003, **103**, 1793–1874, DOI: 10.1021/cr990029p.

37 A. Savin, R. Nesper, S. Wengert and T. F. Fässler, ELF: The Electron Localization Function, *Angew. Chem., Int. Ed. Engl.*, 1997, **36**, 1808–1832, DOI: 10.1002/anie.199718081.

38 T. Novoa, R. Laplaza, F. Peccati, F. Fuster and J. Contreras-García, The NCIWEB Server: A Novel Implementation of the Noncovalent Interactions Index for Biomolecular Systems, *J. Chem. Inf. Model.*, 2023, **63**, 4483–4489, DOI: 10.1021/acs.jcim.3c00271.

39 C. Guerra, J. Burgos, L. Ayarde-Henríquez and E. Chamorro, Formulating Reduced Density Gradient Approaches for Noncovalent Interactions, *J. Phys. Chem. A*, 2024, **128**, 6158–6166, DOI: 10.1021/acs.jpca.4c01667.

40 J. P. Perdew, R. G. Parr, M. Levy and J. L. Balduz, Density-Functional Theory for Fractional Particle Number: Derivative Discontinuities of the Energy, *Phys. Rev. Lett.*, 1982, **49**, 1691–1694, DOI: 10.1103/PhysRevLett.49.1691.

41 R. G. Pearson, *Chemical Hardness*, Wiley, 1997, DOI: 10.1002/3527606173.

42 R. G. Parr, L. v. Szentpály and S. Liu, Electrophilicity Index, *J. Am. Chem. Soc.*, 1999, **121**, 1922–1924, DOI: 10.1021/ja983494x.

43 L. R. Domingo, P. Pérez and J. A. Sáez, Understanding the local reactivity in polar organic reactions through electrophilic and nucleophilic Parr functions, *RSC Adv.*, 2013, **3**, 1486–1494, DOI: 10.1039/C2RA22886F.

44 F. M. Güiza, Y. A. Rodríguez-Núñez, D. Ramírez, A. R. Romero Bohórquez, J. A. Henao, R. A. Toro, J. M. Delgado and G. Díaz de Delgado, Crystal structure, Hirshfeld surface analysis, and molecular dynamics simulations of two isostructural N-propargyl-4-(2-oxopyrrolidin-1-yl)-1,2,3,4-tetrahydroquinolines, *J. Mol. Struct.*, 2022, **1254**, 132280, DOI: 10.1016/j.molstruc.2021.132280.

45 B. Vahdani Alviri, M. Pourayoubi, A. Saneei, M. Keikha, A. van der Lee, A. Crochet, A. A. Ajees, M. Nečas, K. M. Fromm, K. Damodaran and T. A. Jenny, Puckering behavior in six new phosphoric triamides containing aliphatic six- and seven-membered ring groups and a database survey of analogous ring-containing structures, *Tetrahedron*, 2018, **74**, 28–41, DOI: 10.1016/j.tet.2017.11.030.

46 Y. Ouzidan, B. Ş. Yüksel, Y. Filali Baba, B. Hafez, Y. Kandri Rodi, F. Ouazzani Chahdi, J. T. Mague, A. El Hakmaoui, M. Safi, M. Akssira, E. M. Essassi and H. Elmsellem, Synthesis, crystal structure, DFT calculations and Hirshfeld surface analysis of new 2-oxo-1,2-dihydroquinoline-4-carboxylate derivative, *Chem. Data Collect.*, 2022, **41**, 100902, DOI: 10.1016/j.cdc.2022.100902.

47 P. M. McCosker, N. M. Butler, A. Shakoori, M. K. Volland, M. J. Perry, J. W. Mullen, A. C. Willis, T. Clark, J. B. Bremner, D. M. Guldi and P. A. Keller, The Cascade Reactions of Indigo with Propargyl Substrates for Heterocyclic and Photophysical Diversity, *Chem.–Eur. J.*, 2021, **27**, 3708–3721, DOI: 10.1002/chem.202003662.